ACADEMIC PRESS

Available online at www.sciencedirect.com

SCIENCE DIRECT®

Journal of Sound and Vibration 268 (2003) 947–970

JOURNAL OF SOUND AND VIBRATION

www.elsevier.com/locate/jsvi

Feedback control of flexible four-bar linkages: a numerical and experimental investigation

A. Trevisani*

DTG, Department of Management and Engineering, University of Padova, Stradella S. Nicola 3, 36100 Vicenza, Italy

Received 4 February 2002; accepted 26 November 2002

Abstract

A control scheme for a four-bar linkage with all the links flexible is proposed and tested both numerically and experimentally. The control strategy consists in selecting a reduced number of measurable variables through which performing position and vibration are controlled independently. The controlled variables are the crank angle and the link curvatures, which provide an adequate description of the temporal evolution of the mechanism position and vibrational phenomena. Position control is performed through a proportional integral and differential (PID)-like regulator while proportional controllers are employed to damp the fundamental components of the link oscillations. A force of gravity compensator is introduced to increase the control system performances and appropriate devices are proposed to avoid coupling effects among the controlled variables.

The control scheme is first tested and tuned in simulation, where the dynamic behaviour of the flexible linkage is reproduced through a fully coupled non-linear model based on the finite element theory. The performances of the control scheme are assessed by studying the step response of the closed-loop system. The numerical results attained prove that the proposed control scheme achieves efficient positioning and vibration suppression performances. The experimental validation of the control scheme is carried out on an instrumented prototype of the flexible four-bar linkage. Experimental recordings are in good agreement with the numerical results therefore confirming both the effectiveness of the control scheme and the accuracy of the dynamic model.

1. Introduction

In order to reduce manufacturing costs and increase productivity, automatically controlled machines and robot manipulators are being designed to operate at higher speed and with greater

*Tel.: +39-444-998722; fax: +39-444-998888.
E-mail address: trevisiani@gest.unipd.it (A. Trevisani).

0022-460X/$ - see front matter
doi:10.1016/S0022-460X(03)00376-6

position accuracy. High-speed mechanisms need to employ light-weight links to reduce inertia forces, and consequently driving torque requirements. Light-weight links may however originate vibrational phenomena which are not negligible. The effects of such undesired vibrations can be partially reduced by adopting dynamic models accounting for link flexibility during the simulation and the design process. Nevertheless, active control is often necessary for a further reduction of these effects.

Most researchers' investigations in the field of flexible mechanisms are focused on the definition of accurate mathematical models, both for single-link flexible mechanisms and multi-body systems. Numerous contributions can be found in literature as well as thorough reviews of the early studies [1–3]. The prevalent approach is based on the use of discretization techniques to model the elastic links of a mechanism as discrete systems with a finite number of elastic degrees of freedom, and assumes that the total motion of the system be the superposition of a large-amplitude rigid-body motion and a small-amplitude elastic deformation (vibration). Turcic et al. [4] verified experimentally that accurate dynamic models should include coupling terms representing not only the effect of the rigid-body motion on the elastic motion, as in Ref. [5–8], but also the effect of the elastic motion on the rigid-body motion. Finite-element-based and fully coupled dynamic models for multi-body mechanisms have been proposed for instance by Nagarajan and Turcic [9,10], and Giovagnoni [11].

In the last decades a significant effort has also been directed towards developing control schemes for the efficient positioning and vibration damping of flexible mechanism. The complexity of the analytical models that can accurately reproduce flexible mechanism dynamics makes real-time control a difficult task. Linear control schemes have been widely employed with varying degrees of success. In particular, linear quadratic optimal control strategies have been adopted by several researchers both to control single-link [12–14] and multi-body [15,16] systems. In these works approximate state-space formulations of the dynamic models are used, and the control action is based on the values assumed by the state variables of the system. Zhou et al. [14], Book et al. [15], and Caracciolo et al. [16] assume that full state vectors are available for feedback and report numerical results which refer respectively to a one-link mechanism, a two-link arm, and a four-bar linkage. However the direct measurement of all the state variables of a system is almost always impossible, hence, in order to practically employ such control strategies it is necessary to design an observer which reconstructs the state vector from the values assumed by the sensed output (i.e., the measured variables). The use of a state observer has allowed attaining satisfactory experimental results in the control of a one-link flexible robot through linear quadratic regulators [12,13]. Yet the experimental validation of the control schemes designed following this approach is rather difficult when the complexity of the system increases.

Other linear control strategies have been proposed. A feedforward torque predictor and a position and velocity error feedback regulator are used in Ref. [17] and in Ref. [18] to control respectively the joint position and the tip position of a single-link flexible mechanism. The tip control of a single-link flexible mechanism through conventional PD regulators has also been proposed by Park and Asada [19] along with an actuator relocation method for improving flexible mechanism dynamics. Actually the problem of positioning the actuators and the sensors of a flexible mechanism has aroused considerable interest. Lee and Chen [20], for instance, have suggested an optimal design method, based on an energy minimization criterion, which allows an integrated determination of sensor and actuator locations as well as velocity feedback gain. The

application of smart materials featuring distributed sensors and actuators of flexible link mechanism represents another interesting opportunity. Two recent works adopting this concept are those by Liao and Sung [21] and Choi et al. [22].

Non-linear controllers have been less investigated: an example is in the work by Fung and Chen [23] where a method characterized by discontinuous control action is used to control the crank speed and the vibrational phenomena of a slider–crank mechanism with a flexible connecting rod. The use of adaptive control system [24] and of a neural network [25] have also been proposed for the control of single-link flexible mechanisms, while more recently satisfactory experimental results have been achieved by Park et al. [26] in the control of a single-link flexible robot arm with a voice coil-type actuator. The authors suggest using an hybrid control scheme combining fuzzy logic and H_∞ control.

The above references are by no means a complete listing. They are nevertheless representative of the research conducted to date in the field of flexible mechanism position and vibration control. So far the synthesized control schemes have been tested chiefly numerically and on simple mechanisms, which are either single link mechanisms or multi-body systems with usually only one flexible link. Very little is currently present in literature as regards position and vibration control of mechanisms with two or more flexible links, and in particular of closed chain-mechanisms.

The primary objective and contribution of the research described in this paper are to design and test, both numerically and experimentally, a control scheme for a four-bar linkage with all the links flexible. The main problem to be faced when similar mechanisms are considered is that the dynamic models which can represent effectively the real systems are too complicated to be used in the implementation of real-time control schemes. In fact, accurate models are always non-linear and need to be linearized about an equilibrium position to design computationally efficient control schemes. Yet, linearized models may provide inaccurate system dynamics descriptions when large-amplitude displacements are considered.

The discrete model adopted in this work is based on the theory proposed in Ref. [11], and experimentally validated in Ref. [11] and [27] with reference, respectively, to a four-bar and a five-bar linkage. In accordance with such theory each flexible link of a mechanism is subdivided into finite elements and an equivalent rigid-link system (ERLS), defined as in Ref. [28], is utilized as a moving reference configuration from which elastic displacements are measured. The global motion of the mechanism is thereby separated into the large-amplitude rigid-body motion of the ERLS and the superimposed small-amplitude motion due to the link elastic deflections. The differential equations of motion are obtained by direct application of the principle of virtual works and include inertia coupling terms which account for the mutual influence between rigid-body motion and vibration.

This theory is employed to reproduce the dynamic behaviour of a flexible four-bar linkage which moves on a vertical plane driven by an electric motor. A five-beam finite-element representation of the mechanism is adopted, which is characterized by 32 state variables. Because of the high number of state variables, and the practical difficulties in designing state observers for non-linear systems, the control strategy proposed in Ref. [29] is adopted: position and vibration control are performed independently by selecting a reduced number of controlled variables providing a satisfactory description of the mechanism rigid-body motion and vibrational phenomena. In Ref. [29] it is proved, only numerically and referring to the case study reported in Ref. [11], that the simultaneous position and vibration control of a flexible four-bar linkage is

feasible through standard regulators if appropriate devices are adopted to avoid coupling effects among the controlled variables. Moreover a parameter tuning procedure is suggested and the system performances at different sampling times are tested in simulation.

On the basis of the results achieved in Ref. [29], in this paper a control scheme is synthesized for the studied flexible four-bar linkage. The scheme consists of a set of separated controllers operating simultaneously. Position control is performed by means of a regulator derived from a classical PID controller; the controlled variable is the crank angle measured at the motor shaft. A force of gravity compensator is also employed to increase position control performance. Vibration control is achieved through independent proportional regulators, feeding back link curvature signals. The objective is to suppress the highest amplitude oscillations of the mechanism links, which are associated to the link first natural frequencies. All the regulators comprising the control scheme operate simultaneously and effectively because suitable devices are adopted to reduce coupling effects among the controlled variables and to achieve stability. An experimental validation of the control scheme is carried out on a prototype of the flexible linkage. The linkage is driven by a brushless motor, a simplified dynamic model of which is introduced in the simulator, and instrumented so as to measure the desired controlled variables. The control scheme is first tested and tuned in simulation by studying the dynamic response of the closed-loop system to a step input. The numerical results attained prove that the proposed control scheme achieves efficient positioning and vibration suppression performances. The experimental results confirm the effectiveness of the control scheme and are in good correspondence with the numerical results, therefore proving the accuracy of the analytical model in reproducing the fundamental dynamics of the linkage.

2. Dynamics of a flexible link mechanism

2.1. Kinematic relations

The following kinematic definitions are adopted for the ith element and with respect to a common fixed reference frame $\{X, Y, Z\}$: $\mathbf{u}_i$ is the nodal displacement vector, $\mathbf{b}_i$ is the nodal position vector, $\mathbf{r}_i$ is the nodal position vector for the corresponding element of the ERLS, $\mathbf{v}_i$ is the displacement vector of a generic point of the element, $\mathbf{p}_i$ is its position vector, and $\mathbf{w}_i$ is the position vector of the corresponding point in the ERLS. It holds that

$$\mathbf{b}_i = \mathbf{r}_i + \mathbf{u}_i, \quad \mathbf{p}_i = \mathbf{w}_i + \mathbf{v}_i. \tag{1,2}$$

The definitions mentioned are schematically summarized in Fig. 1, where a planar case is considered in accordance with the case study. As it is shown in the figure, beside the fixed reference frame, a local coordinate system $\{x_i, y_i, z_i\}$ is associated with the ith element and follows the motion of the ERLS, whose position is defined by the generalized coordinates contained in a vector denoted $\mathbf{q}$.

The position and orientation of every local system can be uniquely determined through the ERLS kinematics. The position of the ERLS, as well as its velocity and acceleration, can be defined according to the ordinary rules adopted for analyzing rigid-link mechanisms. In

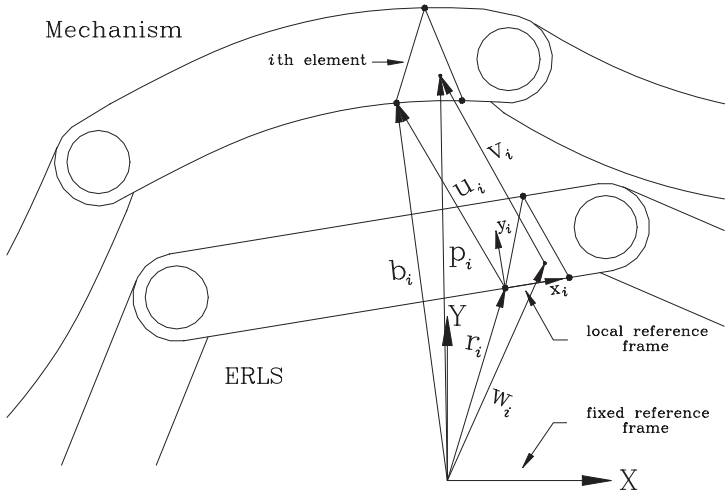

Fig. 1. Kinematic definitions.

particular, by making use of the sensitivity coefficient concept, it is possible to write

$$\mathrm{d}\mathbf{r} = \mathbf{S}(\mathbf{q})\mathrm{d}\mathbf{q}, \quad \dot{\mathbf{r}} = \mathbf{S}(\mathbf{q})\dot{\mathbf{q}}, \quad \ddot{\mathbf{r}} = \mathbf{S}(\mathbf{q})\ddot{\mathbf{q}} + \dot{\mathbf{S}}(\mathbf{q},\dot{\mathbf{q}})\dot{\mathbf{q}} = \mathbf{S}(\mathbf{q})\ddot{\mathbf{q}} + \left(\sum_k \dot{\mathrm{q}}_k \partial\mathbf{S}(\mathbf{q})/\partial \mathrm{q}_k\right)\dot{\mathbf{q}}, \qquad (3-5)$$

where $\mathbf{S}(\mathbf{q})$, is the sensitivity coefficient matrix for all the nodes of the ERLS, and vector $\mathbf{r}$ accounts for the positions of all the nodes of the ERLS ($\mathbf{r}_i$ is a subset of $\mathbf{r}$). If, accordingly, the positions and the elastic displacements of all the nodes are grouped into unique vectors, after differentiating Eq. (1) and employing Eq. (3), the infinitesimal nodal displacement vector $\mathrm{d}\mathbf{b}$ becomes

$$\mathrm{d}\mathbf{b} = \left[\mathbf{I} \,\vdots\, \mathbf{S}\right] \begin{bmatrix} \mathrm{d}\mathbf{u} \\ \hdashline \mathrm{d}\mathbf{q} \end{bmatrix}, \qquad (6)$$

where $\mathbf{I}$ is the identity matrix. The coefficient matrix of the foregoing equation is not square. If e is the dimension of the vector $\mathbf{q}$ of the ERLS generalized coordinates and n is the number of the elastic degrees of freedom contained in vector $\mathbf{u}$, then $\left[\mathbf{I} \,\vdots\, \mathbf{S}\right]$ has n rows and $n+e$ columns. As a consequence a given configuration $\mathrm{d}\mathbf{b}$ of infinitesimal nodal displacements corresponds to more sets of infinitesimal variations $\left[\mathrm{d}\mathbf{u}^{\mathrm{T}} \,\vdots\, \mathrm{d}\mathbf{q}^{\mathrm{T}}\right]$ of the generalized coordinates of the system. To eliminate this redundancy the coefficient matrix must be square, which can be obtained forcing to zero e elements of $\mathrm{d}\mathbf{u}$. By doing so, the position of the ERLS with respect to the actual deformed mechanism is defined univocally. If $\mathrm{d}\mathbf{u}$ is partitioned into its independent part ($\mathrm{d}\mathbf{u}_{in}$) and into its zeroed part ($\mathrm{d}\mathbf{u}_0$), and if $\mathbf{S}$ is correspondingly partitioned, the removal from Eq. (6) of the elements forced to zero allows writing

$$\mathrm{d}\mathbf{b} = \begin{bmatrix} \mathbf{I} & \mathbf{S}_{in} \\ \hdashline 0 & \mathbf{S}_0 \end{bmatrix} \begin{bmatrix} \mathrm{d}\mathbf{u}_{in} \\ \hdashline \mathrm{d}\mathbf{q} \end{bmatrix}. \qquad (7)$$

As pointed out in Ref. [11], a correct ERLS definition requires not only that the square matrix of coefficients of Eq. (7) be non-singular, but also that the generalized co-ordinates of the ERLS be chosen so as to avoid encountering singular configuration during the motion.

The finite element theory is employed to compute the virtual displacement and the real acceleration of a generic point within an element, which are to be determined to apply the principle of virtual work. If $\mathbf{N}_i(x_i, y_i, z_i)$ denotes the shape function matrix of the ith element, Eq. (2) can be rewritten as

$$\mathbf{p}_i = \mathbf{w}_i + \mathbf{R}_i(\mathbf{q})\mathbf{N}_i(x_i, y_i, z_i)\mathbf{T}_i(\mathbf{q})\mathbf{u}_i. \tag{8}$$

$\mathbf{N}_i$ is commonly defined in the local reference frame of the ith element, hence two matrices are introduced in Eq. (8) to perform co-ordinate transformations: $\mathbf{T}_i(\mathbf{q})$ is a block-diagonal matrix expressing the transformation from the global reference frame to the local one of the ith element; $\mathbf{R}_i(\mathbf{q})$ is a matrix expressing the local-to-global transformation.

Virtual displacements ($\delta\mathbf{p}_i$) can be obtained by taking variations of Eq. (8). Both the virtual elastic displacements of the nodes ($\delta\mathbf{u}_i$) and the virtual displacements of the generalized co-ordinates ($\delta\mathbf{q}$) are considered. Moreover the requirement of completeness (which the elements must satisfy to encounter monotonic convergence to the exact solution as the number of elements is increased) allows employing the shape function matrices not only to compute elastic displacements inside the elements but also to represent rigid-body displacements. The following equation is obtained from the complete expression of $\delta\mathbf{p}_i$ by neglecting the terms with the lowest order of magnitude and is employed to interpolate virtual displacements from

$$\delta\mathbf{p}_i = \mathbf{R}_i(\mathbf{q})\mathbf{N}_i(x_i, y_i, z_i)\mathbf{T}_i(\mathbf{q})\delta\mathbf{r}_i + \mathbf{R}_i(\mathbf{q})\mathbf{N}_i(x_i, y_i, z_i)\mathbf{T}_i(\mathbf{q})\delta\mathbf{u}_i. \tag{9}$$

An analogous reasoning allows obtaining the following simplified expression of the acceleration from the complete expression of $\ddot{\mathbf{p}}_i$:

$$\begin{aligned}\ddot{\mathbf{p}}_i = {} & \mathbf{R}_i(\mathbf{q})\mathbf{N}_i(x_i, y_i, z_i)\mathbf{T}_i(\mathbf{q})\ddot{\mathbf{r}}_i + \mathbf{R}_i(\mathbf{q})\mathbf{N}_i(x_i, y_i, z_i)\mathbf{T}_i(\mathbf{q})\ddot{\mathbf{u}}_i \\ & + 2\left[\dot{\mathbf{R}}_i(\mathbf{q})\mathbf{N}_i(x_i, y_i, z_i)\mathbf{T}_i(\mathbf{q}) + \mathbf{R}_i(\mathbf{q})\mathbf{N}_i(x_i, y_i, z_i)\dot{\mathbf{T}}_i(\mathbf{q})\right]\dot{\mathbf{u}}_i.\end{aligned} \tag{10}$$

The complete expressions of $\delta\mathbf{p}_i$ and $\ddot{\mathbf{p}}_i$, and an investigation of their negligible terms are reported in Ref. [11].

The expressions of real and virtual strains also have to be computed to apply the principle of virtual work, since they allow estimating the elastic contributions to the total virtual work. By letting $\mathbf{B}_i(x_i, y_i, z_i)$ denote the strain–displacement matrix, in the local moving frame

$$\varepsilon_i = \mathbf{B}_i(x_i, y_i, z_i)\mathbf{T}_i(\mathbf{q})\mathbf{u}_i, \quad \delta\varepsilon_i = \mathbf{B}_i(x_i, y_i, z_i)\delta\mathbf{T}_i(\mathbf{q})\mathbf{u}_i + \mathbf{B}_i(x_i, y_i, z_i)\mathbf{T}_i(\mathbf{q})\delta\mathbf{u}_i. \tag{11, 12}$$

2.2. Governing equations of motion

The governing equations of motion are obtained by expressing the dynamic equilibrium of the system through the principle of virtual work. For an undamped system, the virtual works due to the inertial, elastic and external forces should be considered. The total virtual work can be computed summing up the elemental contributions. Thus

$$\sum_i \int_{v_i} \delta\mathbf{p}_i^{\mathrm{T}}\ddot{\mathbf{p}}_i\rho_i \,\mathrm{d}v + \sum_i \int_{v_i} \delta\varepsilon_i^{\mathrm{T}}\mathbf{D}_i\varepsilon_i \,\mathrm{d}v = \sum_i \int_{v_i} \delta\mathbf{p}_i^{\mathrm{T}}\mathbf{g}\rho_i \,\mathrm{d}v + (\delta\mathbf{u}^{\mathrm{T}} + \delta\mathbf{r}^{\mathrm{T}})\mathbf{f}, \tag{13}$$

where v_i denotes the ith element volume, ρ_i is the mass density for the element, $\mathbf{D}_i$ is the stress–strain matrix, $\mathbf{g}$ is the gravity acceleration vector, $\mathbf{f}$ is the vector of the concentrated external forces and torques applied to all the nodes of the model, and the virtual displacements $\delta\mathbf{u}$ and $\delta\mathbf{r}$ refer to all the nodes of the model. Invoking the virtual displacement theory, Eq. (13) can be split into two independent equation as

$$\sum_i \delta\mathbf{u}_i^{\mathrm{T}}\mathbf{M}_i(\ddot{\mathbf{r}}_i + \ddot{\mathbf{u}}_i) + 2\sum_i \delta\mathbf{u}_i^{\mathrm{T}}\mathbf{M}_{Gi}\dot{\mathbf{u}}_i + \sum_i \delta\mathbf{u}_i^{\mathrm{T}}\mathbf{K}_i\mathbf{u}_i = \sum_i \delta\mathbf{u}_i^{\mathrm{T}}\mathbf{f}_{gi} + \delta\mathbf{u}^{\mathrm{T}}\mathbf{f}, \tag{14}$$

$$\sum_i \delta\mathbf{r}_i^{\mathrm{T}}\mathbf{M}_i(\ddot{\mathbf{r}}_i + \ddot{\mathbf{u}}_i) + 2\sum_i \delta\mathbf{r}_i^{\mathrm{T}}\mathbf{M}_{Gi}\dot{\mathbf{u}}_i + \sum_i \mathbf{u}_i^{\mathrm{T}}\delta\mathbf{\Phi}_i\mathbf{K}_i\mathbf{u}_i = \sum_i \delta\mathbf{r}_i^{\mathrm{T}}\mathbf{f}_{gi} + \delta\mathbf{r}^{\mathrm{T}}\mathbf{f}, \tag{15}$$

where the Eqs. (9)-(12) are employed and the following definitions, described in detail in Ref. [11], are introduced for the ith element:

$$\int_{v_i} \mathbf{T}_i^{\mathrm{T}}\mathbf{N}_i^{\mathrm{T}}\mathbf{R}_i^{\mathrm{T}}\mathbf{R}_i\mathbf{N}_i\mathbf{T}_i\rho_i\,\mathrm{d}v = \mathbf{M}_i, \quad \int_{v_i} \mathbf{T}_i^{\mathrm{T}}\mathbf{B}_i^{\mathrm{T}}\mathbf{D}_i\mathbf{B}_i\mathbf{T}_i\,\mathrm{d}v = \mathbf{K}_i,$$
$$\int_{v_i} \mathbf{T}_i^{\mathrm{T}}\mathbf{N}_i^{\mathrm{T}}\mathbf{R}_i^{\mathrm{T}}\mathbf{g}\rho_i\,\mathrm{d}v = \mathbf{f}_{gi} \tag{16-18}$$

$$\int_{v_i} (\mathbf{T}_i^{\mathrm{T}}\mathbf{N}_i^{\mathrm{T}}\mathbf{R}_i^{\mathrm{T}}\dot{\mathbf{R}}_i\mathbf{N}_i\mathbf{T}_i + \mathbf{T}_i^{\mathrm{T}}\mathbf{N}_i^{\mathrm{T}}\mathbf{R}_i^{\mathrm{T}}\mathbf{R}_i\mathbf{N}_i\dot{\mathbf{T}}_i)\rho_i\,\mathrm{d}v = \mathbf{M}_{Gi},$$
$$\delta\mathbf{T}_i^{\mathrm{T}} = \delta\mathbf{\Phi}_i\mathbf{T}_i^{\mathrm{T}}. \tag{19, 20}$$

When the elastic displacements are small in comparison with the link dimensions, the term $\sum_i \mathbf{u}_i^{\mathrm{T}}\delta\mathbf{\Phi}_i\mathbf{K}_i\mathbf{u}_i$ of Eq. (15) becomes negligible, because its order of magnitude is much smaller than that of the other terms. Therefore, if Eq. (3) is employed to express the ERLS virtual displacements by means of the sensitivity coefficient matrix, and if unit virtual displacements are imposed, the following expressions holds in terms of assembled matrices and vectors:

$$\mathbf{M}(\ddot{\mathbf{r}} + \ddot{\mathbf{u}}) + (2\mathbf{M}_G + \beta\mathbf{M} + \gamma\mathbf{K})\dot{\mathbf{u}} + \mathbf{K}\mathbf{u} = \mathbf{f}_g + \mathbf{f}, \tag{21}$$

$$\mathbf{S}^{\mathrm{T}}\mathbf{M}(\ddot{\mathbf{r}} + \ddot{\mathbf{u}}) + (2\mathbf{S}^{\mathrm{T}}\mathbf{M}_G + \beta\mathbf{S}^{\mathrm{T}}\mathbf{M})\dot{\mathbf{u}} = \mathbf{S}^{\mathrm{T}}(\mathbf{f}_g + \mathbf{f}), \tag{22}$$

where the Rayleigh coefficients β and γ multiplying the mass and the stiffness matrix have been introduced to take into account damping forces. Finally, by making use of Eq. (5) and by gathering into vector $\mathbf{t} = \mathbf{t}(\dot{\mathbf{u}}, \dot{\mathbf{q}}, \mathbf{u}, \mathbf{q})$ all the forces excluding those directly related to the second derivatives of the generalized co-ordinates, Eqs. (21) and (22) can be grouped together and rearranged in matrix form as

$$\left[\begin{array}{c|c} \mathbf{M}_{in} & (\mathbf{MS})_{in} \\ \hline (\mathbf{S}^{\mathrm{T}}\mathbf{M})_{in} & \mathbf{S}^{\mathrm{T}}\mathbf{M}\mathbf{S} \end{array}\right]\left[\begin{array}{c} \ddot{\mathbf{u}}_{in} \\ \hline \ddot{\mathbf{q}} \end{array}\right] = \left[\begin{array}{c} \mathbf{t}_{in} \\ \hline \mathbf{S}^{\mathrm{T}}\mathbf{t} \end{array}\right] \tag{23}$$

Eq. (23) only includes the nodal elastic displacements which are not forced to zero, and the corresponding matrix elements. Inertia coupling between the accelerations of the ERLS generalized co-ordinates and the elastic accelerations is accounted for through the elements of the submatrices $(\mathbf{MS})_{in}$ and $(\mathbf{S}^{\mathrm{T}}\mathbf{M})_{in}$. Hence, the mutual influence between rigid-body motion and

vibration is taken into consideration: the dynamic behaviour of the ERLS is not independent from vibration and vice versa.

3. Model of the flexible four-bar planar linkage

The above equations of motion are derived for general mechanisms and elements. In this work they have been employed to develop a finite element computer code for the dynamic analysis and simulation of planar elastic mechanisms modelled with classical two-node and six-degree-of-freedom beam elements. The shape function ($\mathbf{N}_i$), mass ($\mathbf{M}_i$), and stiffness ($\mathbf{K}_i$) matrices for two-dimensional Euler beam elements are common knowledge. The Coriolis matrix ($\mathbf{M}_{Gi}$) can be effectively computed through the antisymmetric inertia matrix described in Ref. [8].

The finite element code has been written using Matlab and has been implemented as a *S*-function in order to allow its incorporation into Simulink models. Simulink provides a number of efficient solvers for stiff problems which can be employed for the numerical integration of Eq. (23).

Through the implemented code it has been possible to simulate the dynamic response of the flexible mechanism shown in Fig. 2. The mechanism is a planar four-bar linkage with all the links flexible except for the ground link. A brushless servomotor connected to the fixed frame drives the mechanism, which moves on a vertical plane. The links are straight and slender steel bars with a square cross-section. All the link lengths are different to make it possible to distinguish the link vibration frequencies in the system response. The crank of the mechanism (link1) is screwed into an aluminum wheel (A) rigidly connected to the motor shaft through a collar. Direct coupling of

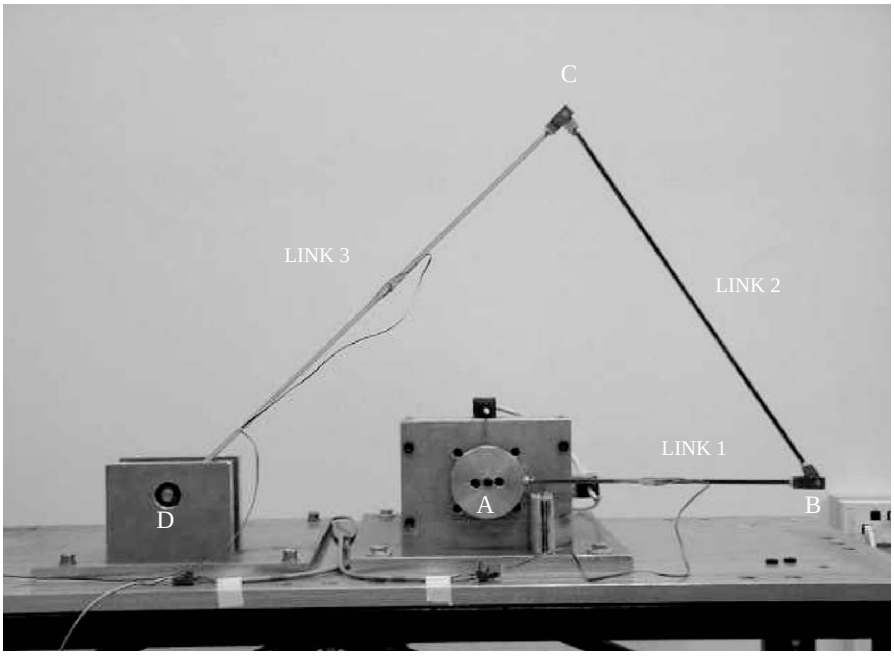

Fig. 2. Front view of the flexible-link planar four-bar linkage.

the motor shaft to the mechanism crank has been preferred in order to prevent the non-linear dynamic phenomena introduced by reduction gears. The kinematic couplings at joints B and C are made of steel roller bearings with negligible clearance and friction losses; the links are tightly screwed into these joints. The revolute joint in D is created by means of a steel shaft supported by two self-aligning ball bearings, whose outer rings are rigidly connected to the fixed frame. A threaded hole has been made on the shaft to allow screwing the follower (link 3). Friction losses in the ball bearings may reasonably be neglected as well as clearance. Further details concerning the experimental apparatus are reported in Section 5.

Fig. 3 illustrates the finite element model of the elastic four-bar mechanism. The model is comprised of five beam elements, and eight nodes: two elements of the same length are used to model links 2 and 3 while for link 1, which is the shortest, a single beam element is employed. Lumped masses are used to account for the moving joints B and C, whose inertias are neglected because of their small dimensions. A concentrated inertia at joint A accounts for the inertia of the brake and the rotor of the brushless motor, and for the inertia of the aluminum wheel and collar. Another concentrated inertia in D accounts for the moving parts of the revolute joint fixed to the frame. The 15 elastic degrees of freedom of the model are shown in Fig. 3, as well as the generalized co-ordinate q (the crank angle) of the ERLS. The dynamic model has therefore 16 degrees of freedom. The elastic degree of freedom forced to zero to define the position of the ERLS with respect to the deformed mechanism is the horizontal displacement at joint C. This definition of the ERLS meets the requirement defined in the previous section for a correct ERLS definition. The same discrete model making use of five beam elements has been employed for a similar four-bar linkage in Ref. [11]. Such work proves that the model gives an accurate prediction of the fundamental dynamics of the mechanism, which depends on the large-amplitude rigid-body

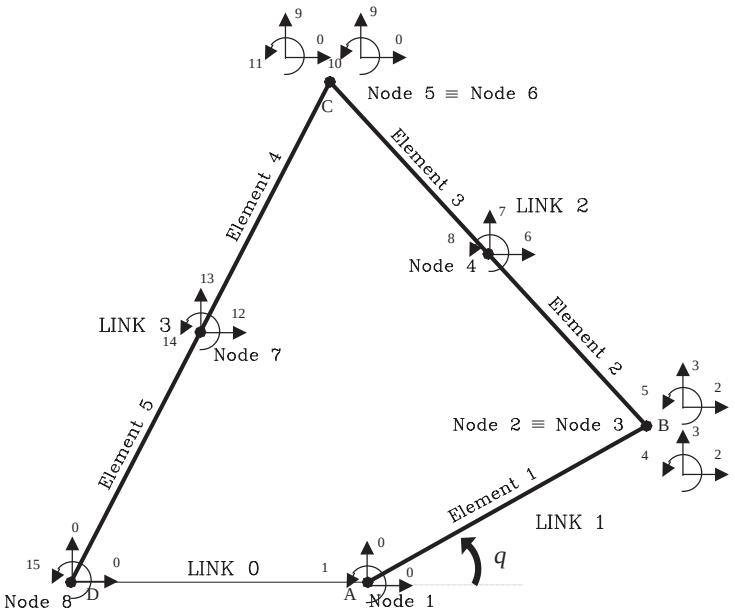

Fig. 3. Finite element model of the flexible-link planar four-bar linkage.

motion of the mechanism and on its primary elastic modes, coinciding approximately with the first modes of the single links, considered pinned–pinned slender beams.

4. Controller design

4.1. Control approach

If one denotes $\mathbf{z} = [\dot{\mathbf{u}}_{in}, \dot{\mathbf{q}}, \mathbf{u}_{in}, \mathbf{q}]$ the state vector of a system modelled by the differential equations of motion (23), on the basis of the considerations made in the previous section, it can be inferred that the studied flexible-link planar four-bar linkage has 32 state variables. Such a high number of state variables makes it impossible to instrument the mechanism so as to get a direct measurement of $\mathbf{z}$. Moreover the classical feedback control techniques developed to design state observers cannot be applied because the mechanism dynamic model is non-linear.

In this work the design of the control system prescinds from the knowledge of the state vector and has been carried out synthesizing independent regulators for position and vibration control. The approach to be followed is based on the selection of a reduced number of controlled variables, which can be easily measured experimentally, and provide an adequate description of the temporal evolution of the mechanism position and of the vibrational phenomena.

4.2. Controlled variables

Different controlled variables are employed by the position and vibration regulators. The proposed dynamic model splits the global motion of the flexible mechanism into two separated, superimposed, and coupled motions: the large-amplitude rigid-body motion of the ERLS, which basically outlines the position of the mechanism, and the small-amplitude elastic motion of the links, which essentially describes the vibrational phenomena. The selected controlled variables for rigid-body and elastic motion control are, respectively, the crank angle and the curvatures of the links. There follows a description of the reasons for the choice.

A complete description of the ERLS motion is provided by its generalized co-ordinate q. This co-ordinate cannot be measured directly, since the position of the ERLS is defined zeroing an elastic degree of freedom of the mechanism model. However, when large displacements of the mechanism are considered and under the hypothesis of small elastic deflections of the links, it can be assumed that q coincide with the crank angle α measured at joint A (see Fig. 3), which is the sum of q and the elastic angular displacement ϕ_1 at node 1.

The angle α can be measured by means of an optical encoder sensing the angular position of the motor shaft. In this work the use of a brushless motor simplifies the apparatus: the motor drive delivers the motor shaft angular position converted to a digital form simulating the output of an incremental encoder.

Because the mechanism links are slender beam-like bars and no external forces acts on the mechanism, apart from gravity loads and the driving torque applied by the motor at one end of the crank, the axial strains in the links are negligible in comparison with transverse deflections. By monitoring the link curvatures it is therefore possible to get an adequate description of the elastic deformations, and consequently of the vibrational phenomena.

Eq. (11) expresses the relation between strain distribution $\boldsymbol{\varepsilon}_i$ in the ith element and the elastic displacements $\mathbf{u}_i$ at the nodes. For the six-degree-of-freedom Euler beam elements employed to model the mechanism links, the small strain theory assumes that axial displacements are independent of transverse displacements and that strains are expressed in terms of axial strains and curvatures. The curvature of the ith element at a particular position can therefore be computed by means of Eq. (11). The curvature is a component of vector $\boldsymbol{\varepsilon}_i$ which is a function of the space co-ordinates.

The curvature of a link can be measured experimentally by means of calibrated strain gages. On every link, the curvature should be measured in the location where it reaches the highest amplitude. By doing so, the possibility of detecting even small elastic deflections is guaranteed during the experiments, and the effect of signal noise on the measurements made by the strain gages is kept to a minimum. The choice of most suitable location is driven by the dynamic behaviour of the links which has been investigated through the mathematical model. The curvatures of links 2 and 3 (C_2 and C_3) are measured at the bar midpoints since these links are characterized by a dynamic behaviour very similar to that of a pinned–pinned beam. As for link 1, since it is the crank of the mechanism, a location closer to joint A has been chosen to measure the curvature (C_1): such a location is at 40% of the link total length.

4.3. Control scheme

The synthesized control scheme consists of a set of separated feedback regulators operating simultaneously and designed for an unrelated control of the mechanism rigid-body motion and vibrations. The control signal is the torque (M) applied by the motor to the mechanism, and it is obtained by summing the contributions of all the independent components of the scheme. The simultaneous use of all the regulators comprising the control scheme is made possible by some appropriate devices which have been introduced to reduce coupling effects among the controlled variables.

4.3.1. Position control

Position (rigid-body motion) control is performed by means of a PID-like regulator. The controlled variable is the crank angle α, which is required to follow an externally-set path over time.

The controller employed is based on a classic PID regulator which is modified to increase performance, reduce sensitivity to vibrational phenomena, and achieve stability. As a matter of fact, inertia coupling between rigid-body motion and vibrations prevents an effective utilization of standard PID regulators, mainly because of the high sensitivity of the derivative action to fluctuations in the value of the position error ($e(t)$). A considerable reduction of the effects of vibrations on the derivative of the position error (velocity error: $\dot{e}(t)$) is obtained by using the transfer function

$$D(s) = s/(1 + sT_c), \tag{24}$$

to compute the Laplace transform of the velocity error while attenuating unwanted error signal components above the cut-off frequency ($1/T_c$). The derivative control therefore provides the following contribution to the overall control signal by

$$M_d = K_d \mathscr{L}^{-1}[D(s)\mathscr{L}[e(t)]], \tag{25}$$

where the symbol $\mathscr{L}$ denotes the Laplace transform of a function. In order to avoid that a high derivative action determines an excessive perturbation of the system when the position reference changes abruptly, a limit is imposed on the absolute value of the derivative signal ("derivative saturation") such that

$$|\dot{e}(t)| = \left|\mathscr{L}^{-1}[D(s)\mathscr{L}[e(t)]]\right| \leqslant S_1. \tag{26}$$

If the angular displacement which the crank undergoes is high in comparison with the vibration amplitude, which is often the case when flexible linkages are considered, the effects of vibrations on the proportional control are generally negligible. No filters are therefore used for smoothing the position error signal, and the following standard relation is employed for computing the contribution of the proportional control to the overall control signal

$$M_p = K_p e(t). \tag{27}$$

For the same reason no filtering of unwanted signals is adopted in the integral-mode controller. The approximate discrete-time expression utilized for calculating the integral of the error signal is

$$\int_0^\tau e(t)\,\mathrm{d}t = T\sum_{j=1}^{k} e_j, \tag{28}$$

where T is the time between successive measurements of the controlled variable (sampling time), e_j is the value of the position error computed at the jth time interval, k is the time interval within which the instant τ falls. The following relation is therefore employed for computing the contribution of the integral control to the overall control signal at the kth time interval, namely

$$M_i^k = K_i T\sum_{j=1}^{k} e_j. \tag{29}$$

In order to make integral control perform effectively, bounds have been imposed on the range of the error calculated at each sampling interval ("input saturation") and on the summation of all errors ("output saturation"):

$$\left|e_j\right| \leqslant S_2, \quad \left|\sum_{j=1}^{k} e_j\right| \leqslant S_3. \tag{30, 31}$$

These bounds reduce the effect of the integral control on the system transient response thus permitting increase of the value of the integral constant and consequently improving the system stability at steady state. Moreover the use of the limitation defined by Eq. (31) increases the integral control reactivity to changes in the position error sign.

Finally, so as to increase the efficiency of the position regulator, the influence of the force of gravity on the mechanism has been compensated separately by computing the value of the torque that counteracts gravity at each angular position α. To compute such a torque is a straightforward kinetostatic problem, whose solution is contained in Ref. [29].

4.3.2. Vibration control

Vibration control is performed by means of autonomous proportional regulators whose controlled variables are the link curvatures. The vibration control problem is subdivided into a set

of independent regulation problems: the objective is the prompt decrease to zero of the amplitude of the elastic oscillations measured on each link.

The values about which link curvature signals oscillate depend on the mechanism position (because the mechanism is under the influence of gravity) and on the torque applied by the motor at each time. However, in order to get accurate information concerning the vibrational phenomena, curvature signals should be processed so as to remove low frequency components and hence to isolate the oscillations at the system natural frequencies. This is basically a data detrending problem which has been solved by subtracting from the actual curvature value, the moving average of the previous values, computed over a fixed number of samples (n). Further details can be found in Ref. [29]. The use of a data detrending filter generates a short delay that only affects the mean value of the curvature but not the amplitude and the frequency content of the elastic oscillations.

Let $\bar{C}_{ik}$ denote the value of the ith link curvature estimated at the kth time interval, the contribution to the overall control signal provided by the proportional regulator of the ith link is computed as follows:

$$M_{ci}^{k} = K_{ci}\bar{C}_{ik}. \tag{32}$$

Fig. 4 shows a block diagram of the synthesized control scheme where all the independent regulators are represented. It is noticable that, as far as vibration control is concerned, the controlled variables are C_1 and C_3. No vibration control is provided for the second link (the coupler) since a strain gage carrier amplifier with just two-channels was available for this experimental investigation. Actually the coupler oscillations are negligible in comparison with those of the other two links, owing to the mechanism geometry and the case study chosen to assess the control scheme performance.

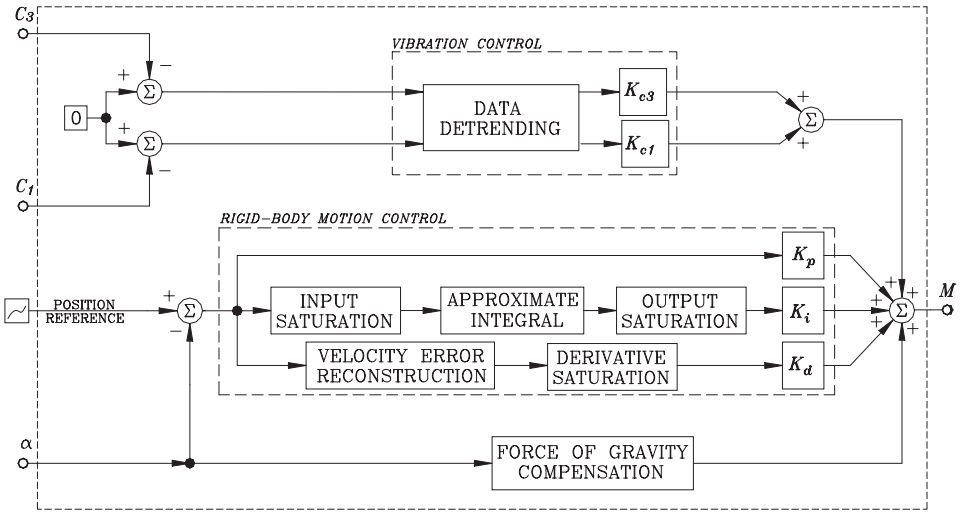

Fig. 4. Block diagram of the control scheme.

5. Case study

Table 1 reports the geometric and inertial characteristics of the flexible link mechanism to which the theory developed in the foregoing sections has been applied. A first description of the mechanism has been provided in Section 3. Additional information is concerning the driving motor, the instruments used for measuring the values of the controlled variables, and the controller follows.

The brushless motor is an Indramat type MKD with a maximum torque of 11 N m. The motor operating mode is set to torque regulation with analog interface (± 10 V) in accordance with the features of the control scheme designed. The motor shaft angular position (α), is delivered directly by the motor drive with a resolution of 2.197×10^{-2} degrees, and read by a 24-bit encoder card.

Half-bridge strain gages are located on the crank and on the follower at the positions set in Section 4.2, and are calibrated for measuring the link curvatures in the plane of motion. The signals produced by the strain gage bridges are conditioned by a HBM MGC carrier with two one-channel amplifier modules. To eliminate measurement noise and to prevent aliasing problems, the strain-gage signals are passed through a low-pass filter having a Butterworth characteristic and a cut-off frequency of 1000 Hz. Analog signals from the carrier are acquired by means of a 12-bit ADC/DAC card. The same card is also employed to generate the analog input of the motor drive.

The control scheme is implemented and run on a PC where a real-time kernel that interfaces with the operating system is installed through The MathWorks Real-Time Windows Target. In order to prevent aliasing problems, the sampling time adopted is 2 ms, corresponding to a frequency of 500 Hz, approximately six and a half times higher than the maximum frequency measured (see Table 2).

Table 1
Mechanical parameters of the prototype

Link	0: Ground	1: Crank	2: Coupler	3: Follower
Length (m)	0.3588	0.3728	0.5250	0.6320
Width (m)	–	6×10^{-3}	6×10^{-3}	6×10^{-3}
Thickness (m)	–	6×10^{-3}	6×10^{-3}	6×10^{-3}
Total mass (kg)	–	0.1014	0.1413	0.1801
Flexural stiffness: EJ (N m^2)	–	21.6	21.6	21.6
Joint	**A**	**B**	**C**	**D**
Lumped mass (kg)	–	72.4×10^{-3}	71.3×10^{-3}	–
Concentrated inertia (kg m^2)	490×10^{-6}	–	–	120×10^{-7}

Table 2
First natural frequencies of links 1 and 3

First natural frequency (Hz)	Link 1	Link 3
Numerical results	76.17	36.13
Experimental results	75.92	35.88

The control scheme has been first tested and tuned in simulation by studying the step response of the closed-loop system: starting from the equilibrium configuration in which the crank is horizontal ($\alpha = 0^\circ$), the controlled variable α is required to follow a reference path characterized by a step change of 45° taking place at time 0.1 s. The values of the regulator parameters have been determined so as to meet the dynamic performance requirements defined in terms of time response specifications as

$$\text{setting time of } \alpha: \ < 0.8\,\text{s}, \ \text{overshoot of the final value of } \alpha: \ < 15\%,$$

and to ensure an effective reduction of the amplitudes of the link elastic oscillations, while keeping the maximum value of the control signal below the torque limit of the brushless motor adopted.

6. Numerical results

The dynamic simulator of the complete experimental apparatus comprises the model of the four-bar flexible linkage described in Sections 2 and 3, and a simplified model of the driving motor on the basis of the motor operating mode, the ratio of the torque exerted to the signal voltage applied to the input terminal of the motor drive is assumed to be constant, at any position and rotational speed. The motor inertial characteristics are accounted for in the dynamic model of the mechanism through the concentrated inertia at joint A (Table 1). Moreover, a first order low-pass filter with a cutoff radian frequency of 250 rad/s, is introduced to reproduce the attenuation of the high frequency components of the position feedback signal delivered by the motor drive. The value of the cut-off frequency has been determined experimentally through an identification procedure. The simulated signals of the controlled variables and the control signal have been sampled at 500 Hz to match the experimental conditions.

The parameters of the position and the vibration controllers have been tuned separately, by adopting a procedure similar to the one described in Ref. [29]. No optimization techniques have been employed to improve the value chosen, since determining the best values for the parameters is beyond the scope of this work. Table 3 reports the values of the parameters which have allowed meeting the performance requirements defined in the previous section.

The time-histories of the controlled variables and of the control signal computed analytically carrying out the experiment with the controller parameter values set as in Table 3 are plotted as

Table 3
Controller parameters

Position control		Vibration control	
K_p	480×10^{-6}	K_{c1}	12
K_d	140×10^{-6}	K_{c3}	60
S_1 (sectors/s)	12×10^3	n (samples)	35
T_c (s)	5×10^{-2}		
K_I	1.5×10^{-2}		
S_2 (sectors/step)	5		
S_3 (sectors/step)	150		

solid lines in the Figs. 5–8. The major features of the system step response are reported in Table 4 and are inferred from the time-history of the crank angle α plotted in Fig. 5. The time-histories of the link curvatures C_1 and C_3 are shown in Figs. 6 and 7, where a shorter time scale is adopted to for clarity.

The comparison of the aforementioned time-histories with those plotted as dashed line, which are obtained without vibration control (i.e., setting $K_{c1} = K_{c3} = 0$ and the position control

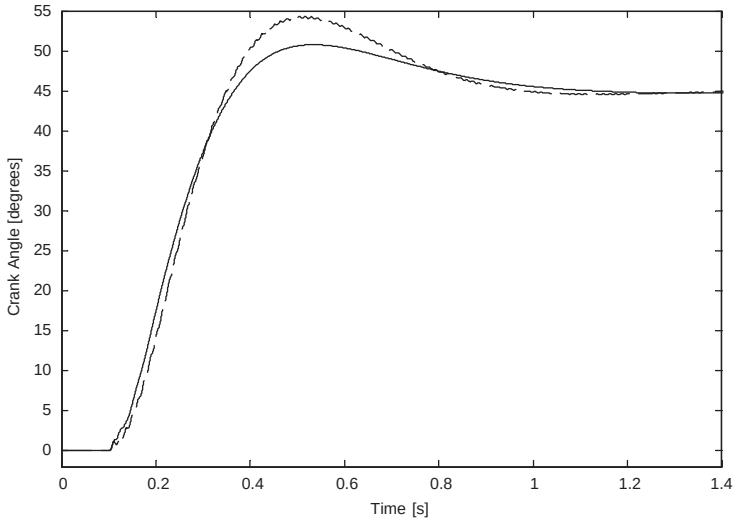

Fig. 5. Comparison of the crank angles computed analytically with (solid line) and without (dashed line) vibration control.

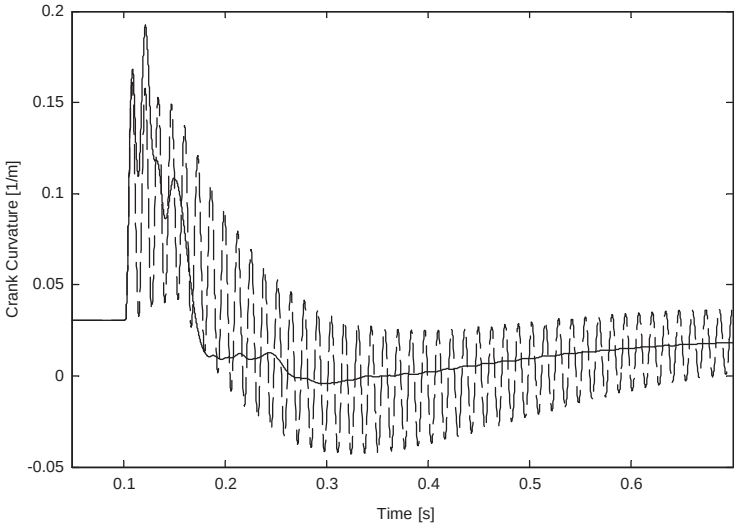

Fig. 6. Comparison of the crank curvatures computed analytically with (solid line) and without (dashed line) vibration control.

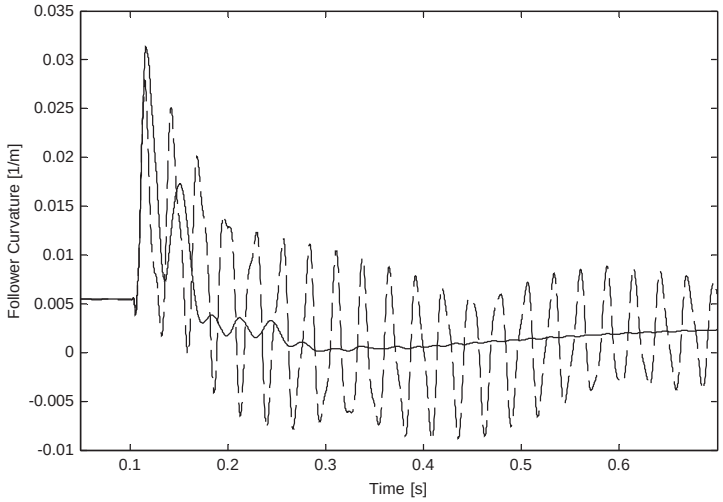

Fig. 7. Comparison of the follower curvatures computed analytically with (solid line) and without (dashed line) vibration control.

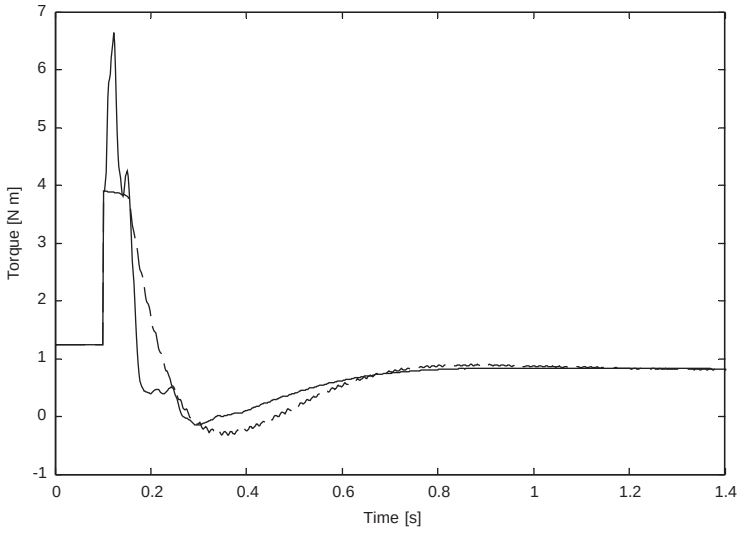

Fig. 8. Comparison of the driving torques computed analytically with (solid line) and without (dashed line) vibration control.

parameters as in Table 3), demonstrates the effectiveness of the control scheme. In fact, when no vibration control is performed, oscillations of a not negligible amplitude are clearly visible not only in the link curvature plots, but also in the crank angle plot. The fundamental components of the motion of the crank and the follower are at the frequencies reported in Table 2. These frequencies are mean frequencies during the motion because they slightly change in virtue of the change in the boundary conditions of the links. Having introduced simple Rayleigh damping in

Table 4
Major features of the system dynamic response

	Numerical results	Experimental results
Overshoot of the final value	$5.78^\circ \sim 12.84\%$	$2.88^\circ \sim 6.4\%$
Settling time ($\pm 5\%$)	0.718 s	0.482 s
Transient rise time (10–90%)	0.180 s	0.186 s
Response time (50%)	0.122 s	0.116 s

the numerical model ($\beta = 8.7 \times 10^{-2}$ and $\gamma = 4.5 \times 10^{-5}$) the amplitudes of the oscillations decrease gradually, but slowly. Vibration control remarkably reduces the duration of the undesired vibrational phenomena: Figs. 6 and 7 prove that the fundamental components of the oscillations in both the links are damped in about 0.25 s, hence before reaching the target angular position.

Fig. 8 allows comparing the torque computed by the control scheme, and consequently applied to the crank of the mechanism, with and without vibration control. The time-history of the torque computed without vibration control (dashed line) clearly shows both the effect of the derivative saturation immediately after the step change occurs, and the persisting oscillations of the torque values at the crank first natural frequency. These oscillations disappear when vibration control is performed (solid line). The additional contribution provided by the vibration controller greatly modifies the control signal, and in particular the maximum value achieved. Such value is considerably higher than the one computed without vibration control, but still below the motor torque limit.

The satisfactory results achieved in simulation highlight that all the controllers can operate simultaneously without interfering significantly, and consequently prove the effectiveness of the devices adopted to avoid coupling effects among variables.

7. Experimental results

A consistent experimental validation of the synthesized control scheme and of the dynamic model adopted is obtained by analyzing the dynamic response of the experimental apparatus to the step input defined previously, and by comparing the experimental recordings with the results achieved in the numerical analysis. Figs. 9–12 include the comparison between the time-histories of the controlled variables and of the control signal recorded experimentally (solid line) and computed in the simulation (dashed line). The experimental investigation is carried out using the same controller parameters employed in the simulation, and reported in Table 3. The main features of the real system step response are reported in the third column of Table 4. They meet the performance requirements defined previously, as well as the maximum torque exerted which is below the motor torque limit.

The numerical results and the experimental recordings are in good agreement, which proves the accuracy of the numerical model and the effectiveness of the control scheme. As a matter of fact the numerical model reproduces accurately the fundamental dynamics of the linkage both when vibration control is performed and when it is not; moreover the fundamental vibrational

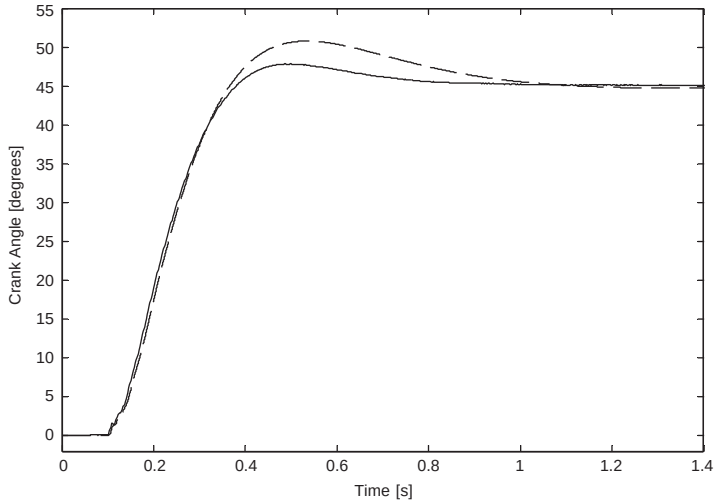

Fig. 9. Comparison of the crank angles recorded experimentally (solid line) and computed analytically (dashed line) with vibration control.

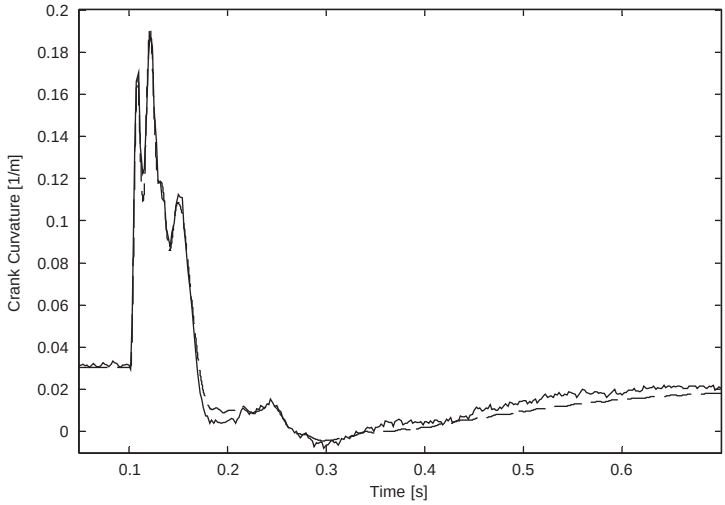

Fig. 10. Comparison of the crank curvatures recorded experimentally (solid line) and computed analytically (dashed line) with vibration control.

phenomena are damped by the control scheme in approximately the same time as in the simulation. The accuracy of the numerical results achieved is also a consequence of the chosen ERLS definition, which minimizes elastic displacements and rotations at the nodes because the crank undergoes large deformations, forcing to zero the horizontal elastic displacement at joint C is a better choice than forcing to zero the elastic rotation at the motor shaft as in Ref. [8].

Fig. 9 and Table 4 show that the real system performs better than was predicted by the numerical model, both the settling time and the overshoot values are lower. Only negligible differences can be discriminated in the time-histories of the link curvature values (Figs. 10 and 11),

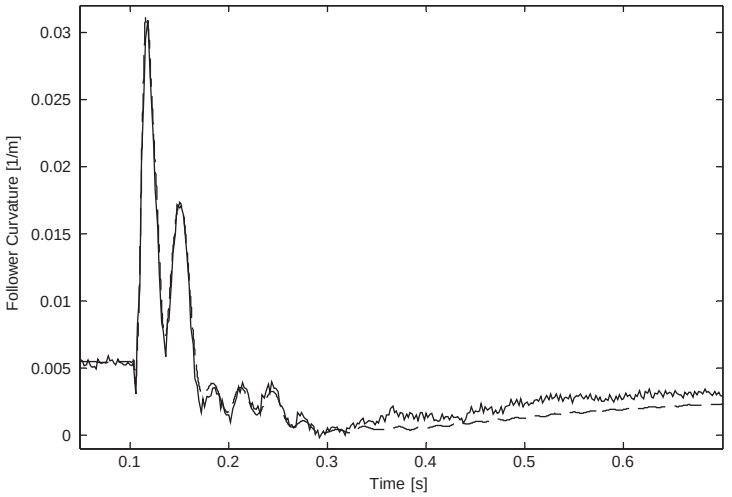

Fig. 11. Comparison of the follower curvatures recorded experimentally (solid line) and computed analytically (dashed line) with vibration control.

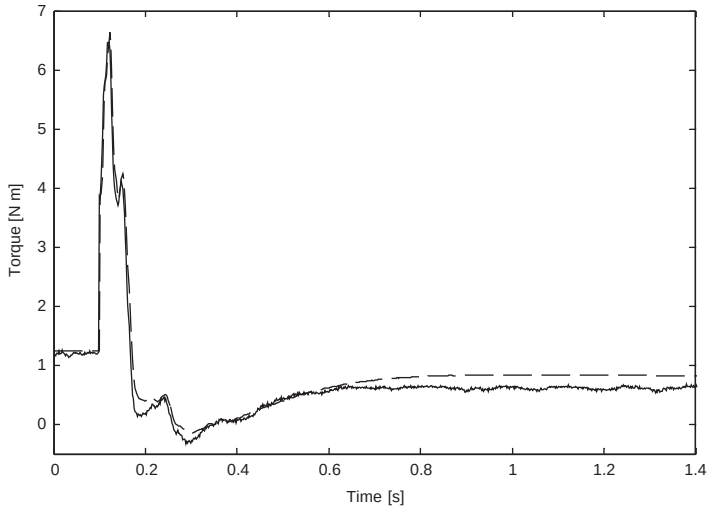

Fig. 12. Comparison of the driving torques recorded experimentally (solid line) and computed analytically (dashed line) with vibration control.

while the different torque values keeping the mechanism in equilibrium at the target position in the simulated and the experimental tests are referable to the simplifying assumptions in the dynamic model concerning the mechanism geometric and inertial characteristics.

Spectrum analyses of the curvature waveforms recorded when no vibration control is performed have allowed identifying the frequency of the fundamental component of each signal. These frequencies are reported in the third row of Table 2. They are slightly lower than those predicted by the theoretical model, which yields a stiffer idealized system compared to the actual system. This is in accordance with the principles of the finite element theory. Figs. 13 and 14 allow

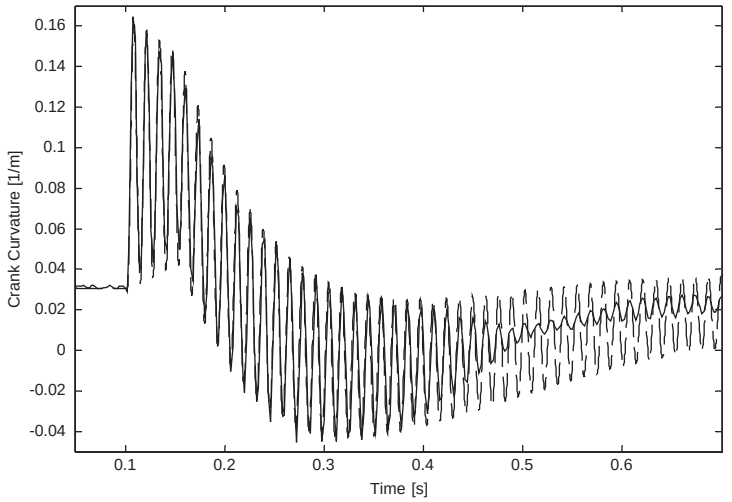

Fig. 13. Comparison of the crank curvatures recorded experimentally (solid line) and computed analytically (dashed line) without vibration control.

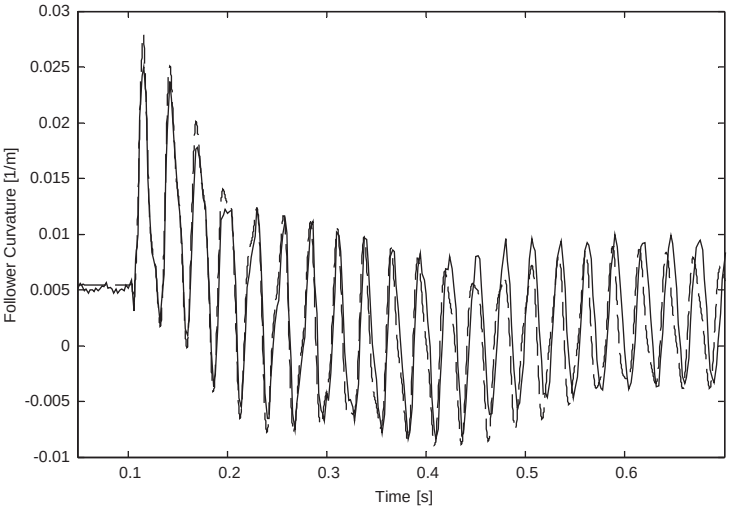

Fig. 14. Comparison of the follower curvatures recorded experimentally (solid line) and computed analytically (dashed line) without vibration control.

comparing link curvatures computed in the simulation and recorded experimentally without vibration control. As can be seen from the plots, the experimental and numerical results show a very good agreement both in terms of frequency and amplitude. Nonetheless an abrupt decrease in the amplitude of the crank vibrations has been recorded experimentally after about 0.35 s since the beginning of the experiment (Fig. 13). Such an unforeseen damping effect can be traced back to the motor dynamics, which is not reproduced with exhaustive accuracy by the simplified model employed in the simulator. The fact that no unexpected decrease in the vibration amplitude can be observed in the time-history of the follower curvature (Fig. 14) corroborates this evidence.

8. Conclusions

In this work a scheme for the position and vibration control of a four-bar linkage with all the links flexible has been designed and tested, both numerically and experimentally.

The control scheme has been first tested and tuned in simulation, where the dynamic behaviour of the flexible linkage is reproduced through an accurate non-linear mathematical model based on the finite element theory. An equivalent rigid-link system (ERLS) is used in the model as a moving reference configuration for elastic displacement measurements. The actual mechanism motion is therefore split into a large-amplitude rigid-body motion with a superimposed small-amplitude elastic motion. The equations of motion are obtained by applying the principle of virtual work and include inertia coupling terms accounting for the mutual influence between rigid-body motion and vibration.

Because of the high number of state variables characterizing the model of the mechanism and the practical difficulties in designing state observers for non-linear systems, a reduced number of easily measurable controlled variables is selected to perform position and vibration control independently. Position control is performed by means of a PID-like regulator; the controlled variable is the crank angle measured at the motor shaft. Vibration control is performed by means of independent proportional regulators; the curvatures of the links are the controlled variables. Moreover, at each position the torque produced by gravity is computed and counteracted by a separate force of gravity compensator. The use of appropriate devices allows partially avoiding coupling effects among the controlled variables therefore permitting the simultaneous use of all the independent feedback regulators.

The performance of the control scheme has been assessed in simulation by studying the step response of the closed-loop system. The numerical results achieved show that the scheme ensures a rapid arrival at the target position and a prompt damping of the undesired vibrational phenomena. The comparison with the results obtained without vibration control proves the effectiveness of the scheme.

An instrumented mechanism prototype has been set up to get a consistent experimental validation of the synthesized control scheme. The experimental step response of the system is in good conformity with the one predicted analytically, which confirms the effectiveness of the control scheme and the accuracy of the dynamic model. In particular, very good agreement has been shown to exist between the frequency content of the experimental and simulated signals of the controlled variables. However when no vibration control is performed some discrepancies have arisen between the amplitudes of the oscillations of the crank curvature values. It is quite likely that a more accurate mathematical model of the brushless motor driving the mechanism could improve the above comparisons attenuating the remaining discrepancies.

References

[1] G.G. Lowen, W.G. Jandrasits, Survey of investigations into the dynamic behavior of mechanism containing links with distributed mass and elasticity, Mechanism and Machine Theory 7 (1972) 3–17.

[2] A.G. Erdman, G.N. Sandor, Kineto-elastodynamics—a review of the state-of-the-art and trends, Mechanism and Machine Theory 7 (1972) 19–33.

[3] G.G. Lowen, C.C. Chassapis, The elastic behavior of linkages: an update, Mechanism and Machine Theory 21 (1986) 33–42.
[4] D.A. Turcic, A. Midha, J.R. Bosnik, Dynamic analysis of elastic mechanism systems. Part II: experimental results, American Society of Mechanical Engineers, Journal of Dynamic Systems, Measurement and Control 106 (1984) 255–260.
[5] W.L. Cleghorn, B. Taborrok, R.G. Fenton, Finite element analysis of high-speed flexible mechanisms, Mechanism and Machine Theory 16 (1981) 407–424.
[6] W. Sunada, S. Dubowsky, The application of finite element methods to the dynamic analysis of flexible spatial and co-planar linkage systems, American Society of Mechanical Engineers, Journal of Mechanical Design 103 (1981) 643–651.
[7] D.A. Turcic, A. Midha, Generalized equations of motion for the dynamic analysis of elastic mechanism systems, American Society of Mechanical Engineers, Journal of Dynamic Systems, Measurement and Control 106 (1984) 242–248.
[8] D.A. Turcic, A. Midha, Dynamic analysis of elastic mechanism systems. Part I: applications, American Society of Mechanical Engineers, Journal of Dynamic Systems, Measurement and Control 106 (1984) 249–254.
[9] S. Nagarajan, D.A. Turcic, Lagrangian formulation of the equations of motion for elastic mechanisms with mutual dependence between rigid body and elastic motions. Part I: element level equations, American Society of Mechanical Engineers, Journal of Dynamic Systems, Measurement and Control 112 (1990) 203–214.
[10] S. Nagarajan, D.A. Turcic, Lagrangian formulation of the equations of motion for elastic mechanisms with mutual dependence between rigid body and elastic motions. Part II: systems equations, American Society of Mechanical Engineers, Journal of Dynamic Systems, Measurement and Control 112 (1990) 215–224.
[11] M. Giovagnoni, A numerical and experimental analysis of a chain of flexible bodies, American Society of Mechanical Engineers, Journal of Dynamic Systems, Measurement and Control 116 (1994) 73–80.
[12] R.H. Cannon, E. Schmitz, Initial experiments on the end-point control of a flexible one-link robot, International Journal of Robotic Research 3 (1984) 62–75.
[13] R. Caracciolo, E. Ceresole, M. Giovagnoni, Control experiment of a flexible robot arm using the floating frame model, Journal of Robotics and Mechatronics 8 (1996) 112–121.
[14] P. Zhou, F.Y. Wang, W. Chen, P. Lever, Optimal construction and control of flexible manipulators: a case study based on LQR output feedback, Mechatronics 11 (2001) 59–77.
[15] W.J. Book, O. Miazza-Neto, D.E. Whitney, Feedback control of two beams, two joint system with distributed flexibility, American Society of Mechanical Engineers, Journal of Dynamic Systems, Measurement and Control 97 (1975) 424–431.
[16] R. Caracciolo, A. Gasparetto, A. Rossi, A. Trevisani, Linear quadratic optimal control of a planar four-link flexible linkage, Proceedings of the Iasted International Conference "Robotics and Applications 2000", Honolulu, HI, 2000.
[17] A.A. Goldenberg, F. Rakhsha, Feedforward control of a single-link flexible robot, Mechanism and Machine Theory 21 (1986) 325–335.
[18] A. Shchuka, A.A. Goldenberg, Tip control of a single-link flexible arm using a feedforward technique, Mechanism and Machine Theory 24 (1989) 439–455.
[19] J.H. Park, H. Asada, Dynamic analysis of noncollocated flexible arms and design of torque transmission mechanism, American Society of Mechanical Engineers, Journal of Dynamic Systems, Measurement and Control 116 (1994) 201–207.
[20] A.C. Lee, S.T. Chen, Collocated sensor/actuator positioning and feedback design in the control of flexible structure system, American Society of Mechanical Engineers, Journal of Vibration and Acoustics 116 (1994) 146–154.
[21] C.Y. Liao, C.K. Sung, An elastodynamic analysis and control of flexible linkages using piezoceramic sensors and actuators, Journal of Mechanical Design 115 (1993) 658–665.
[22] S.B. Choi, C.C. Cheong, B.S. Thompson, M.V. Gandhi, Vibration control of flexible linkage mechanisms using piezoelectric films, Mechanism and Machine Theory 29 (1994) 535–546.
[23] R.F. Fung, H.H. Chen, Dynamic analysis and vibration control of a flexible slider-crank mechanism using PM synchronous servo motor drive, Journal of Sound and Vibration 214 (1998) 605–637.

[24] R.I. Milford, S.F. Asokanthan, Experimental on-line frequency domain identification and adaptive control of a flexible slewing beam, American Society of Mechanical Engineers, Journal of Dynamic Systems, Measurement and Control 118 (1994) 58–65.
[25] K. Takahashi, I. Yamada, Neural-network based learning control of flexible mechanism with application to a single-link flexible arm, American Society of Mechanical Engineers, Journal of Dynamic Systems, Measurement and Control 116 (1994) 792–795.
[26] H.W. Park, H.S. Yang, Y.P. Park, S.H. Kim, Position and vibration control of a flexible robot manipulator using hybrid controller, Robotics and Autonomous System 28 (1999) 31–41.
[27] R. Caracciolo, A. Gasparetto, A. Trevisani, Experimental validation of a dynamic model for flexible link mechanisms, Proceedings of the American Society of Mechanical Engineers DETC, Pittsburgh, PA, USA, 2001.
[28] L.W. Chang, J.F. Hamilton, The kinematics of robotic manipulators with flexible links using an equivalent rigid link system (ERLS) model, American Society of Mechanical Engineers, Journal of Dynamic Systems, Measurement and Control 113 (1991) 48–53.
[29] R. Caracciolo, A. Trevisani, Simultaneous rigid-body motion and vibration control of a flexible four-bar linkage, Mechanism and Machine Theory 36 (2001) 221–243.